Journal of
Materials Chemistry C

Accepted Manuscript

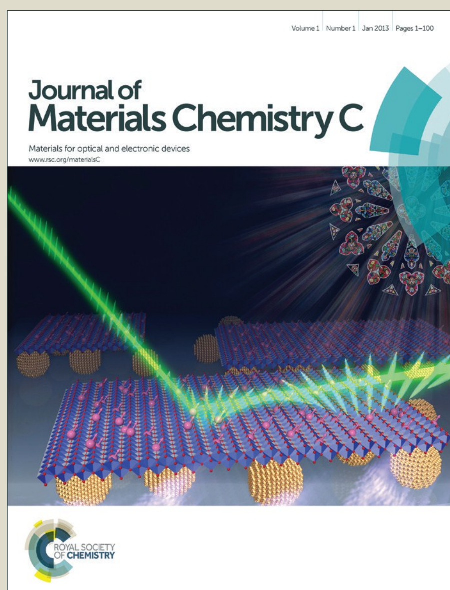

This is an *Accepted Manuscript*, which has been through the Royal Society of Chemistry peer review process and has been accepted for publication.

Accepted Manuscripts are published online shortly after acceptance, before technical editing, formatting and proof reading. Using this free service, authors can make their results available to the community, in citable form, before we publish the edited article. We will replace this *Accepted Manuscript* with the edited and formatted *Advance Article* as soon as it is available.

You can find more information about *Accepted Manuscripts* in the Information for Authors.

Please note that technical editing may introduce minor changes to the text and/or graphics, which may alter content. The journal's standard Terms & Conditions and the Ethical guidelines still apply. In no event shall the Royal Society of Chemistry be held responsible for any errors or omissions in this *Accepted Manuscript* or any consequences arising from the use of any information it contains.

ROYAL SOCIETY
OF CHEMISTRY

www.rsc.org/materialsC

Journal Name

ARTICLE

Solution processable amorphous hafnium silicate dielectrics and its application for oxide thin film transistors

Received 00th January 20xx,
Accepted 00th January 20xx

DOI: 10.1039/x0xx00000x

www.rsc.org/

Y. N. Gao,[a] Y. L. Xu, [a] J. G. Lu[b], J. H. Zhang[a] and X. F. Li*[a]

Abstract: A novel solution-processed amorphous high-*k* dielectric for thin film transistors (TFTs) has been systemically studied with the objective of achieving high performance and reducing costs for the next generation displays. In this research, the amorphous hafnium silicon multiple oxide (HfSiOx) was fabricated by the simple spin-coating method. Here, we have demonstrated that the incorporation of a silicon oxide has significant effects on the properties of HfO_2. The HfSiOx dielectrics have no obvious crystallization peaks even the annealing temperature reach up to 800 ºC while the HfO_2 films were crystallized at 400 ºC. The HfSiOx films have an energy band gap of 6.05 eV, which was wider than HfO_2 films (5.69 eV), the breakdown voltage was increased from 2.4 MV/cm (HfO_2) to 2.9 MV/cm (HfSiOx) and the leakage current was decreased from 4.4×10^{-7}A/cm^2 to 3.7×10^{-7}A/cm^2 at an electric field of 2 MV/cm. To achieve optimized device performance, the influence of annealing temperature on the characteristics (including the surface and interface, the chemical and structural evolution) of the solution processed HfSiOx dielectrics was emphasized in this research. To demonstrate the HfSiOx application on oxide TFTs, we fabricated HfInZnO (HIZO) and ZnSnO (ZTO) TFTs with HfSiOx dielectrics, and both of them showed low off-state current indicating the HfSiOx is an attractive candidate used in TFTs. The ZTO TFTs with amorphous HfSiOx dielectrics were operated well under a gate voltage of -0.53 V, exhibiting a high saturation mobility of 153 cm^2/V·s, a small subthreshold swing of 0.17 V/dec, a large on-off current ratio 3.4×10^7.

1. Introduction

Transparent amorphous oxides semiconductors (AOS) thin film transistors (TFTs) have been extensively investigated for potential application in the large size active matrix flat panel display (AMFPD) owing to their excellent optical transparency, high carrier mobility and electrical stability [1-3]. Along with the rapid development of the AMFPD technology, high resolution and low power consumption with low operating voltage is desirable for battery-powered and portable applications. To reduce the operation voltage of TFTs, one can either reduce the thickness of the gate dielectric layer or use the high dielectric constant (high-*k*) gate dielectric. However, the thickness reduction of the traditional dielectric layer (SiO_2 or SiN_x) will inevitably result in the increase of gate leakage current due to direct tunneling. Hence, to solve this problem, high-*k* oxide materials such as HfO_2[4], ZrO_2 [5], TiO_2 [6] and Ta_2O_3[7] which can simultaneously enable low tunneling leakage current through the use of thicker films, as well as low-voltage operation have been studied.

However, most of high-*k* oxides have a tendency to crystallize at a relative low process temperature (400 ºC) and produce grain boundaries [4, 5]. It would lead to electrical leakage current and increase the gate leakage current of TFTs which may lead to high off-state current, low on/off current ratios and increased power consumption[8]. Moreover, the grain boundary of crystalline structure in the high-*k* dielectric would affect the film uniformity and induce variations in device to device performance. Also, the high-*k* dielectrics generally have a lower optical energy bandgap (*Eg*) and smaller band offsets relatively to the semiconductor than conventional SiO_2/SiNx, decreasing the device breakdown voltage[9]. Eventually, all of these could result in an inferior dielectric reliability. Thus, it is necessary to exploit different amorphous high-*k* and high *Eg* dielectric oxides to meet the future demands of flat plate display industry.

To develop amorphous high-*k* dielectric, some research groups have investigated different multicomponent dielectrics based on a mixture of high-*k* dielectrics (ZrO_2, HfO_2, TiO_2) and different dopants, such as Al[10, 11] , La [12] and Si[13-15], to increase the crystalline temperature. Among them, silicon oxide has a wide bandgap, small ion radius and high Si-O band energy. Consequently, the crystalline phase of hafnium silicate (HfSiOx) films was suppressed to 800 ºC[16]. Meanwhile, the energy bandgap of HfO_2 was enlarged and the breakdown voltage was increased owing to the silicon doping. As the previous reported, HfSiOx dielectrics have advantages such as high dielectric constant than SiO_2, a larger band gap than HfO_2[17] and much fewer and weaker traps than HfO_2 which would result in good thermal stability [18]. Thus, it is believed to

a. Key Laboratory of Advanced Display and System Application, Ministry of Education, Shanghai University, Shanghai 200072, China
b. Key Laboratory of Silicon Materials, Department of Materials Science and Engineering, Zhejiang University, Hangzhou 310027, China
*Email: lixifeng@shu.edu.cn
†Electronic Supplementary Information (ESI) available: Supplementary figures See DOI:10.1039/x0xx00000x

Journal of Materials Chemistry C Accepted Manuscript

be a good dielectric candidate in direct contact with Si and can meet requirements for high resolution and low consumption AMFPD display technology[19]. Simultaneously, few groups[17, 13, 20] have demonstrated TFTs based on HfSiOx dielectrics. S. Lee et.al reported pentacene thin film transistors with hafnium silicate fabricated through atomic layer deposition and D. Cho et.al fabricated IZO-based TFTs with HfSiOx gate insulators deposited by co-sputtering.

However, to date, most of HfSiOx dielectrics were fabricated through expensive vacuum-based deposition process such as atomic layer deposition [17, 21, 22], sputtering [13, 20] and electron bean evaporation [23], which suffered from high manufacturing costs and limitation to large area deposition capabilities. To develop HfSiOx films in low cost, using simple methods such as dip coating [24], inkjet printing [25] and spin-coating [10, 11] was promising. Furthermore, current researches of HfSiOx materials were almost only focused on the films or powders [26] properties such as surface and structure, crystallization behaviors, insulating properties and effects of Si concentration [22] and studied in the range of high annealing temperature (> 600 ^{o}C) [27, 28] which are incompatible with transparent electronic technology based on glasses.

Hence, to further improve transparent TFTs devices performance, it is important to develop solution processable HfSiOx dielectrics and verify their characteristics at relative low annealing temperatures (< 600 ^{o}C). In this work, the effects of Si incorporation and annealing conditions on HfSiOx film properties were investigated systemically, including the thermal behavior of HfSiOx solutions, crystallization optical and insulating properties, chemical and structural evolution of HfSiOx films. Based on the investigation on HfSiOx dielectrics, the fabricated processes of solution processed HfInZnO (HIZO) thin film transistors were optimized and improved device performance were obtained. Simultaneously, considering that the earlier studies by Hoffman and co-workers demonstrated that the sputtered ZnSnO (ZTO) TFTs could achieve high mobility (~30 $cm^2/(V\cdot s)$) for the TFTs at the annealing temperatures ranged from 400 ^{o}C to 600 ^{o}C [29] and most of the recent reports on solution processed ZTO TFTs were almost based on SiO_2 dielectrics [30, 31], we also applied HfSiOx dielectrics on ZTO TFTs to verify the properties of HfSiOx dielectrics and further improved the TFTs performance.

2. Experimental

2.1 Precursor Solution Preparation.

The HfSiOx solution was prepared by dissolving hafnium dichloride oxide octa-hydrate ($HfCl_2O\cdot 8H_2O$) and tetraethyl orthosilicate ($Si(OC_2H_5)_4$) into 2-methoxyethanol (2-MOE) successively. 2-MOE was commonly used as the solvent since it can act as a bridging ligand and thus stabilize intermediate high-molecular weight oligomers. The molar composition ratio of the HfSiOx precursor solution was Hf:Si = 2:1. The HfO_2 solution was prepared by dissolving $HfCl_2O\cdot 8H_2O$ into 2-MOE. We used hafnium chloride ($HfCl_4$), zinc acetate dihydrate ($Zn(CH_3COO)_2\cdot 2H_2O$) and indium nitrate hydrate ($In(NO_3)_3\cdot xH_2O$) as the metal precursors of hafnium zinc and indium, respectively. The molar ratio of Hf:In:Zn = 0.2:3:2. For Zinc Tin oxides (ZTO) precursor solution, $Zn(CH_3COO)_2\cdot 2H_2O$ and $SnCl_2\cdot 2H_2O$ were dissolved into 2-MOE, and their molar ratio was Zn:Sn=7:3. The monoethanolamine (MEA) was added as a sol stabilizer after the precursors of HIZO and ZTO were mixed with 2-MOE. The concentration of all the above precursor solutions was 0.3 M and all the solutions were finally stirred for 24 hours at room temperature to form homogeneous colloids.

2.2 Film Preparation.

The HfSiOx solutions were filtered through a 0.22 μm polytetrafluoroethylene (PTFE) syringe filter and then spin-coated on Corning EXG glass substrates with the thickness of 0.7 mm and size of 200 mm × 200 mm or quartz substrate (for measuring *Eg* of films specifically) at 3000 rpm for 50s. The spin-coated HfSiOx films were prebaking at 120 ^{o}C for 15 min to remove the solvent and then annealed at 300 ^{o}C for 30 min in an ambient atmosphere. The spin-coating process was repeated four times to achieve the desired thickness which was about 105 nm after the annealing treatment at 500 ^{o}C. For HIZO or ZTO films, the corresponding precursor solutions were filtered through a 0.22 μm PTFE syringe filter firstly and then spin-coated on Corning EXG glasses in the rotating speed of 3000 rpm. However, the prebaking and annealing temperature for HIZO and ZTO films were 150 and 300 ^{o}C, respectively. The spin-coating process was repeated twice to achieve the desired thickness which was about 35 nm after the annealing treatment at 500 ^{o}C.

2.3 Device Fabrication.

To examine the electrical properties of HfSiOx dielectric, we fabricated metal-insulator-metal structures. First, the HfSiOx films were spin-coated on ITO substrates. Then, the HfSiOx films were annealed at different temperatures (300, 400 and 500 ^{o}C). Finally, circle aluminum electrodes (radius = 0.5 mm) were thermally evaporating via a shadow mask.

Thin film transistors were fabricated on the glass substrates. As shown in the inset of figure 6a, ITO was used as the gate electrodes. The HfSiOx solutions were spin-coated on the prepared substrates. And then ITO was deposited by sputtering and patterned as source and drain electrodes before spin-coated HIZO precursors on the fabricated substrates. However, for ZTO TFTs, ZTO films were deposited before the fabrication of source and drain electrodes (as shown in the inset of figure S7). All the patterns were fabricated through a lithographic process. The width and length of the channel region of the fabricated HIZO/ZTO TFTs were 50 and 10 μm, respectively.

2.4 Film Characterization.

The thermal behavior of HfSiOx solutions monitored under nitrogen atmosphere using thermal gravimetric and differential scanning calorimetry (TG-DSC, SDT Q600) which was operated at temperatures ranging from room temperature to 800 ^{o}C with a scan rate of 10 ^{o}C/min. The surface topography and roughness of HfSiOx films were analyzed by atomic force

Journal of Materials Chemistry C Accepted Manuscript

This journal is © The Royal Society of Chemistry 20xx

microscopy (AFM; Nanonavi SPA-400 SPM). The crystallization and structural information of HfSiOx films was obtained through grazing incidence x-ray diffraction (XRD, D/MAX-2550) with the glancing incident angle of 1°. The film thickness and refractive index were measured by spectroscopic ellipsometry. The chemical and structural properties of HfSiOx dielectrics were examined by X-ray photo-electron spectroscopy (XPS, Thermo ESCALAB 250). The carbon 1s peak at 284.6 eV was used as a reference for calibration in the XPS results. The capacitance-voltage (*C-V*) was measured using an Agilent E4980A precision LCR meter and the capacitance-frequency (*C-f*) was measured by Wayne Kerr 6500B precision impedance analyzer. The dielectric leakage (I_G) and TFT electrical characteristics including transfer and output properties were performed by and Agilent 4155C semiconductor parameter analyzer.

3. Results and discussion

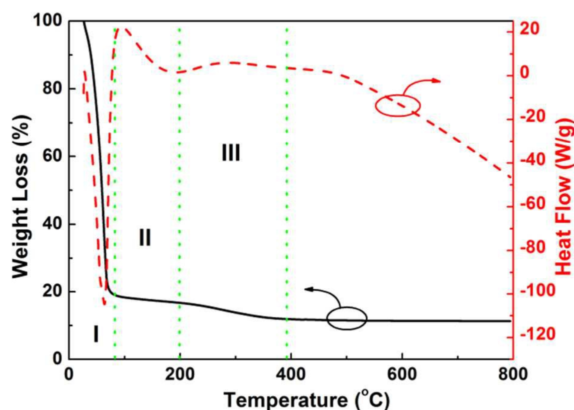

Fig. 1 Thermal gravimetric and differential scanning calorimetry (TG-DSC) curves of HfSiOx solution.

To examine the chemical reactions in the HfSiOx solution, TG-DSC analysis was performed under air atmosphere from room temperature to 800 °C. As shown in figure 1, an exothermic peak near ~70 °C was observed with a large weight loss below 90 °C. This was primarily caused by evaporation of the solvent and hydrolysis of HfSiOx solution. The other broad exothermic peak located at 200-400 °C was corresponding to the gradual condensation behavior, which form the metal-oxygen-metal (M-O-M) frame, decrease the impurities in the film and make dense films [32]. After 395 °C, no significant weight loss was observed, indicating the HfSiOx oxidization behavior was almost completed. Meanwhile, no peaks indicating the crystallization of HfSiOx films were observed even the temperature was up to 800 °C. To confirm the crystallization performance and verify the effects of Si doping on HfSiOx films, we investigate the formation and crystallization of solution processed HfSiOx oxides using XRD detection at various annealing temperatures (300-900 °C).

Figure 2 showed the XRD patterns of HfSiOx films annealed at 800 °C and 900 °C. The XRD patterns of HfSiOx films annealed at temperatures ranged from 300 to 700 °C are shown in figure S1a. The HfSiOx films were amorphous until the annealing temperature of 800 °C. The 900 °C annealed films had a crystalline orhtorhmbic HfO_2 phase (PDF #40-1173) with (012) (101) (103) and (123) peaks at 32, 30.2, 50.5 and 61.2 °. Meanwhile, the peak located at 35.5 ° corresponding to tetragonal Hf_2Si (211) phase (PDF #120467). It is known that HfO_2 crystallize at an annealing temperature of 400 °C[33] (as shown in figure S1b). However, the HfSiOx films had no crystalline peak until 800 °C indicating the Si addition have assistance to blocking the crystallization of the HfO_2 films and forming amorphous structure films. And an amorphous phase is known to be advantageous over a crystalline phase owing to its low leakage current and high breakdown voltage [4]. Compared with the XRD pattern of HfO_2 films (as shown in the inset of figure 2) annealed at 900 °C. The pure HfO_2 crystallized into the monoclinic one (PDF #65-1142). A phase transformation from the monoclinic to orthorhmbic indicating the important effects with Si doping HfO_2 was observed. The trend of this phase transformation is similar to the previous reported HfSiOx films deposited by sputtering [34].

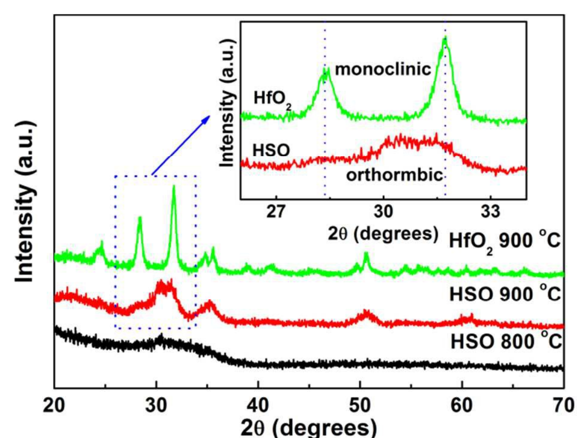

Fig. 2 XRD patterns for HfSiOx annealed at 800 and 900 °C and HfO_2 films annealed at 900 °C.

Figure S2a showed the surface root mean square (RMS) roughness values of HfO_2 and HfSiOx films annealed at different temperatures. And figure S2b was the AFM image of HfSiOx films annealed at 500 °C. Compared with the RMS roughness values of films annealed at 400 and 500 °C, HfSiOx films (0.17 and 0.26 nm) were smoother than HfO_2 films (0.79 and 0.82 nm). This fact was attributed to the combination of silicon oxide with HfO_2. The smoother surface of HfSiOx films would help to reduce the defect density and suppress the charge trapping in the interface between the channel and gate dielectric[7]. The improved interface quality would suppress the leakage current induced by surface roughness and improve the electrical properties [35].

In order to confirm the optical bandgap difference between HfO_2 and HfSiOx films, UV-visible spectroscopy measurement was performed. The transmittance spectra of the intrinsic HfO_2 and HfSiOx films deposited on quartz substrate were shown in figure 3. The thickness of HfO_2 films annealed at 500 °C was about 155 nm and the thickness for HfSiOx films as-coated and

Journal of Materials Chemistry C Accepted Manuscript

annealed at 300, 400, 500 °C were about 333, 230, 200 and 187 nm, respectively. As the annealing temperature increased, the thickness of HfSiOx thin films decreased, which was due to the evaporation of solvent and the densification process of the thin films [36]. The spectra clearly demonstrated high optical transmittance of films. The onset of the optical transitions of the HfO_2 and HfSiOx films near the band edge are illustrated in the inset of figure 3. The optical bandgap (*Eg*) can be obtained by the absorption coefficient (α). α could be obtained by equation 1:

$$\alpha = \frac{1}{d}\ln(\frac{1}{T}) \quad (1)$$

where *d* and *T* represent the film thickness and transmittance, respectively. The optical bandgap can be expressed by the Tuac relation [37]

$$(\alpha h\upsilon)^2 = \mathrm{A}(h\upsilon - Eg) \quad (2)$$

where *h* is Planck's constant, and υ is the photon frequency, A is a constant, and *Eg* is the optical direct band gap. According the transmittance of films and equation 1 and 2, the optical bandgap can be extracted. The HfSiOx films had a wider bandgap of 6.05 eV while the bandgap of HfO_2 was 5.69 eV. It indicated that the addition of Si increased the bandgap of dielectric layer. Thus, the bandgap offsets to the semiconductor was improved relatively which can increase the breakdown voltage and lower the leakage current [9].

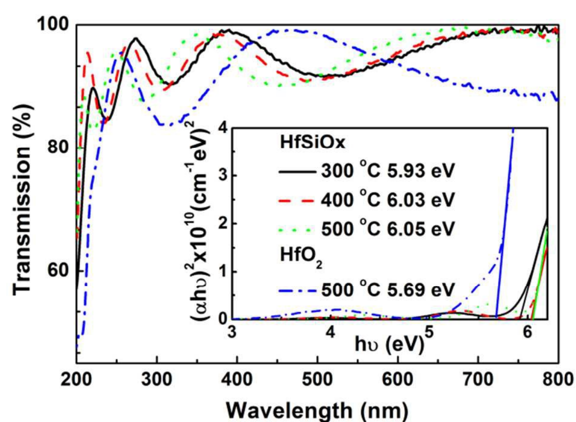

Fig. 3 Transmittance spectra of the HfSiOx and HfO_2 films annealed at different temperatures. The inset was the $(\alpha h\nu)^2$ vs. photo energy plots of the HfSiOx and HfO_2 films annealed at different temperatures.

The transmittance of HfSiOx films annealed at different temperatures was also shown in figure 3. Slight blue shifts in the transmittance of HfSiOx films annealed at 300 to 500 °C were observed. We can calculate the *Eg* from the equation 1 and 2 and the calculated *Eg* were listed in table 1. Obviously, the values of *Eg* were increased with annealing temperatures. At low annealing temperatures, the undecomposed residual solvent including the hydrogen groups and Cl ions or an imperfect M-O-M acting as scatter centers may result in the decrease of film transmittance.

To further verify the Si incorporation effects and the densification behavior of HfSiOx films, spectroscopic ellipsometry measurements were performed. The index of refraction (n) values were summarized in table 1.

For comparison, at 550 nm, the index of refraction (*n*) values of bulk SiO_2 and HfO_2 are 1.54 and 2.1, respectively [38]. In this research, the "*n*" values we measured for HfO_2 and HfSiOx films annealed at 500 °C were 1.748 and 1.872, respectively. According to the Lorentz-Lorenz relation, the refractive index can be related to the evolution of packing density and polarization [39]. Since the Si-O bonds were less polar than the corresponding Hf-O bands [19], the addition of Si would lead to a decrease of the film polarization, and then lowering the refractive index of HfSiOx films [40]. The "*n*" for HfO_2 films were lower than that of bulk, crystalline HfO_2 which may related with the less dense films solution processed. In addition, "*n*" values of HfSiOx films annealed at 300, 400 and 500 °C were 1.698, 1.743 and 1.748 respectively, which is comparable to vacuum-deposited counterparts. The refractive index was increased with the annealing temperature indicating the effect of temperature on enhancing the refractive index and representing a denser HfSiOx film as the annealing temperature increases [4]. However, the increase was slightly when the annealing temperature increased from 400 °C to 500 °C, indicating that the oxidization behavior of HfSiOx films was almost complete. And further improvement or changes may be possible only if the film is fully crystallized or if a structural transformation occurs [41].

Table 1 Summary of the characteristics of HfSiOx and HfO_2 dielectrics annealed at different temperatures.

Temperature (°C)	*Eg* (eV)	*n*	*ε*	Breakdown Voltage (MV/cm)
300 (HfSiOx)	5.93	1.698	10.1	-
400 (HfSiOx)	6.03	1.743	10.6	1.2
500 (HfSiOx)	6.05	1.748	10.8	2.9
500 (HfO_2)	5.69	1.872	13.1	2.4

The chemical compositions of the HfSiOx dielectrics were characterized by XPS and the results were shown in figure 4. Figure 4a showed the Hf 4f XPS spetra of HfO_2 and HfSiOx films annealed at 500 °C. The Hf $4f_{7/2}$ peak of HfO_2 films was located at 18.43 eV with a fully oxidized state of Hf^{4+} and spin-orbit splitting of 1.6 eV from the Hf $4f_{5/2}$ component (figure 4a). The Hf $4f_{7/2}$ and Hf $4f_{5/2}$ peaks in Hf 4f XPS spectra of HfSiOx films were located at 17.29 and 18.69 eV respectively. The binding energy in Hf 4f XPS spectra shifted to higher values when Si was added into HfO_2 oxides. Meanwhile, the O 1s XPS spectra for HfSiOx films also shifted to the higher binding compared with that for HfO_2 films. These effects may be resulted from the difference in electronegativities of Hf and Si (1.9 and 1.3 eV, respectively) [16].

As shown in figure 4c, when the annealing temperature increased, both Hf $4f_{7/2}$ and Hf $4f_{5/2}$ peaks shifted from 17.46 eV and 18.90 eV to 17.29 eV and 18.69 eV, respectively. These results may be related to the progressive oxidization to HfSiOx, which was also described in figure 1 (TGA). Annealing caused

Journal of Materials Chemistry C Accepted Manuscript

This journal is © The Royal Society of Chemistry 20xx

a higher degree of forming Hf-Si bonds, and atoms had sufficient activation energy to reduce the Hf-O bond length. These increased Hf-Si bonds length caused the decrease in binding energy [41]. Moreover, a new peak in the Hf 4f XPS spectra associated with the Hf-Si bonds located at 15.7 eV [19] was observed for HfSiOx films annealed at 400 and 500 °C. As the temperature increased to 400 °C, a new peak occurred in the Si 2p XPS spectra. It located at 98.9 eV and may be related with Hf-Si bond [43]. This result also confirmed the Hf-Si bond exists.

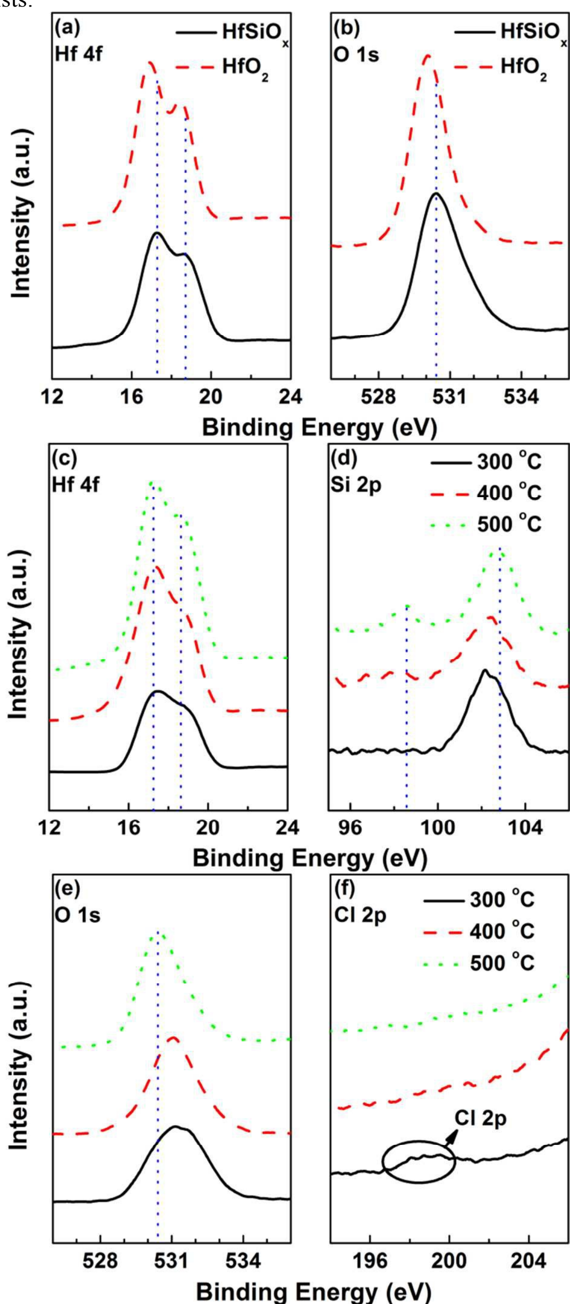

Fig. 4 (a) Hf and (b) O XPS spectra of HfSiOx and HfO_2 films annealed at 500 °C. (c) Hf (d) Si (e) O (f) Cl XPS spectra of HfSiOx films as a function of the annealing temperatures.

And the details of oxidization behavior for HfSiOx films annealed at different temperatures were confirmed by O 1s peaks. The O 1s peaks in the HfSiOx films can be deconvoluted into two peaks corresponding to the OH groups at 532.1 eV (Peak 1), and the fully oxidized state (Peak 2). The area ratio of the peaks was used to estimate the relative quantities of the oxygen lattice and hydroxyl groups. Obviously, the relative areas of the hydroxyl-group-related peak were reduced monotonically with increasing annealing temperature, as shown in Figure 4e and Figure S3. In contrast, the relative area of the oxygen lattice peak was increased with the increase of annealing temperature. Simultaneously, the peak 2 for oxygen lattice shifted from 531 eV to 530.5 eV. In general, these phenomena were attributed to dehydrogenation of HfSiOx films [32]. However, in HfSiOx films research, it may also be related with the generation of Hf-Si bonds, which would lead to a relative increase of the ratio of Hf-O/Si-O bonds. This was in accordance with the analysis of Si 2p and Hf 4f XPS spectra.

The reduction of concentration of Cl ions after annealing is also observed in the Cl 2p spectra. In figure 4f, only the 300 °C annealed HfSiOx films Cl 2p XPS spectra showed a broad peak located at 198.8 eV, indicating it contained the largest concentrations of chlorine and hydroxyl groups. The incomplete decomposition of organic ligands and metal salts due to low annealing temperature is believed to cause the excessive existence of Cl ions and hydroxyl groups (M-OH) [44]. As the annealing temperature was increased, such impurities were reduced substantially with the enhanced decomposition and evaporation. Meanwhile, the M−OH were converted to oxides. Thus, the HfSiOx films became denser and the insulation improved with increasing annealing temperature.

The insulating properties of HfSiOx dielectrics fabricated at different annealing temperatures were examined by fabricating metal-insulator-metal (MIM) structure. The HfSiOx dielectric films were deposited on the ITO/Glass substrate and a circular Al (radius = 0.5 mm) was thermal evaporated as the top electrodes. In the MIM structure, the thickness of HfO_2 films annealed at 500 °C was about 100 nm. And the thickness of HfSiOx films annealed at 300, 400 and 500 °C were about 130, 110 and 105 nm respectively. The gate leakage current density (J_g) versus the applied electric field (E) of the HfSiOx dielectric was shown in figure 5a. In order to compare the J_g values of HfSiOx and HfO_2 films with different annealing temperatures, they were plotted as a function of the thickness normalized electric field.

Figure 5a showed the J_g values for HfSiOx and HfO_2 films, from which it can be seen that, both the HfO_2 and HfSiOx films exhibited low leakage current density, however, the HfO_2 films were broken down at an electric field of 2.4 MV/cm which was lower than that at which the HfSiOx films broken down (2.9 MV/cm). It was caused by the crystallization structure of HfO_2 films annealed at 500 °C. Leakage current density of HfSiOx films was increased with decreasing annealing temperature, likely related to defects associated with incomplete condensation [45]. Residual impurities such as Cl or C ions related organics and hydrogen groups provided the leakage current paths and resulted in the high leakage current densities

Journal of Materials Chemistry C Accepted Manuscript

Please do not adjust margins

of HfSiOx annealed at low temperature (above 10^{-5} A/cm^2 at 1 MV/cm) [36]. When annealing temperature increased to 500 °C, HfSiOx dielectric films showed a low leakage current density (about 10^{-7} at 1MV/cm) and high breakdown voltage (2.9 MV/cm). These results indicated that HfSiOx films annealed at 500 °C were suitable to be a dielectric in thin film transistors [46].

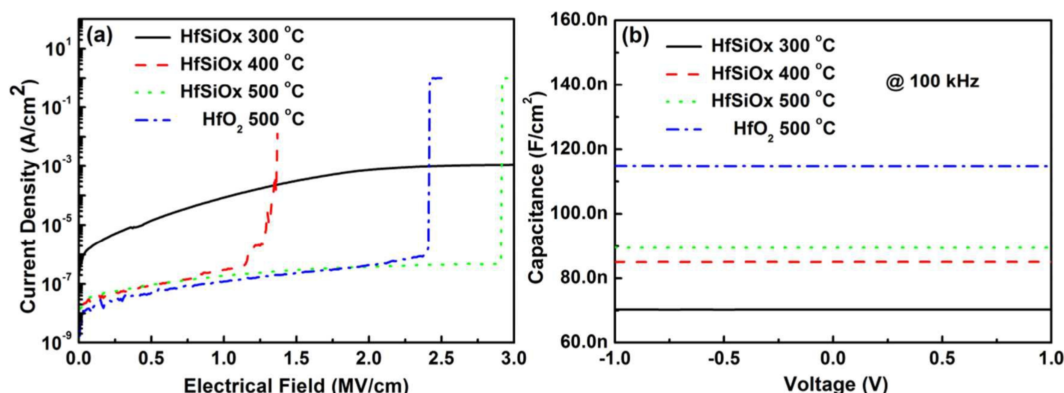

Fig. 5 (a) Leakage current density-Electric field and (b) capacitance-voltage plots of HfSiOx and HfO_2 films annealed at different temperatures.

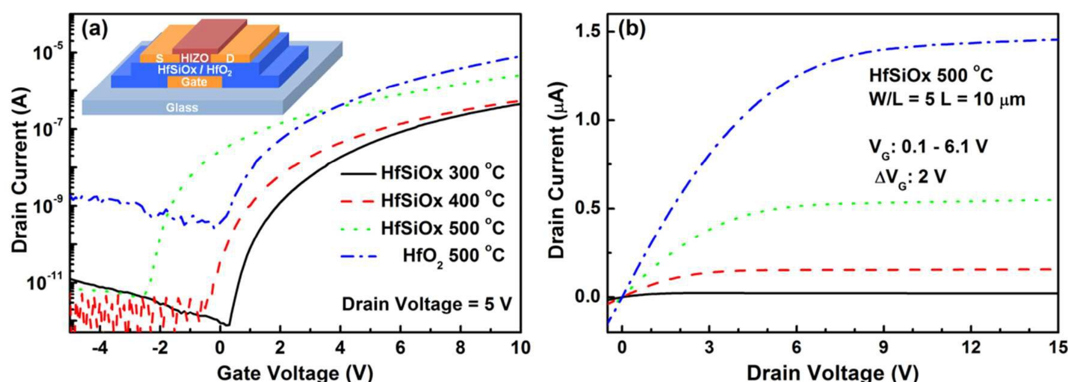

Fig. 6 (a) Transfer characteristics of HIZO TFTs with HfSiOx and HfO_2 dielectrics annealed at different temperatures. (b) Output characteristics of HIZO TFTs with HfSiOx dielectrics annealed at 500 °C. Inset in figure 6a was the structure schematic of the HIZO TFTs.

Table 2 Electrical performance of solution processed TFTs annealed at different temperatures.

TFT type	Temperature (°C)	V_T(V)	μ(cm^2/V·s)	I_{on}/I_{off}	*S.S* (V/dec)
HIZO/HfSiOx	300	2.28	0.78	5.13×10^5	0.97
HIZO/HfSiOx	400	1.30	1.48	2.55×10^5	0.85
HIZO/HfSiOx	500	-1.44	6.11	6.14×10^5	0.55
HIZO/HfO_2	500	0.51	3.64	2.92×10^4	1.1
ZTO/HfSiOx	500	-0.53	153	3.40×10^7	0.17

Capacitance-frequency (*C-f*) measurements were conducted on the same MIM structures employing the HfSiOx dielectric films annealed at different temperatures. As shown in figure S4, HfSiOx films annealed at 300 °C exhibited relatively unstable frequency-dependent characteristics, and their dielectric constants decrease obviously at high frequencies suggesting the poor insulating properties [47]. It was contribute to the residual organics and incomplete oxide lattice formation which was in consistence with poor leakage current and the XPS results. The HfSiOx dielectrics annealed at 300, 400 and 500 °C had capacitances of 69, 85, 91 nF/cm^2 at 100 kHz (as shown in figure 5b), corresponding to dielectric constants of 10.1, 10.6 and 10.8, respectively. The high value of capacitance of low temperature annealed HfSiOx films in the case of low frequency is attributed to the existence of hydroxyl groups. The dielectric constant of HfSiOx films annealed at 500 °C was about 10.8 which was in accordance with the previous reported HfSiOx films fabricated by ALD [17].

To verify the HfSiOx films annealed at 500 °C as a gate dielectric, HIZO TFTs with bottom-gate-bottom-contact

Journal of Materials Chemistry C Accepted Manuscript

 This journal is © The Royal Society of Chemistry 20xx

structures and HfSiOx dielectric were fabricated. For comparison, TFT characteristics with 300 and 400 annealing temperatures are also shown in figure 6a. The performances of all devices were summarized in table 2. The threshold voltage (V_T) was defined as the gate voltage (V_{GS}) that induces a drain current of $L/W \times 10$ nA at $V_{DS} = 5$ V [30]. And the mobility was calculated through the equation as follows:

$$I_{DS} = \frac{WC_i\mu_{sat}}{2L}(V_{GS} - V_T)^2$$

In this equation, the W/L = 5, and the capacitance was measured at 100 kHz which was showed in figure 5b. The saturation mobility (μ_{sat}) was calculated in the region of V_{DS}>V_{GS}-V_T.

TFTs annealed at 300 °C exhibited a saturation mobility of 0.78 cm^2/V·s, a V_T of 2.28 V, a subthreshold swing (*S.S*) of 0.97 V/dec, an on-off current ratio (I_{on}/I_{off}) 5.13×10^5. The HfSiOx dielectric TFTs annealed at 500 °C showed a better performance for increased saturation mobility and lower subthreshold swing as shown in table 2. These temperature-dependence behaviors were related with the reduced impurities and hydrogen groups. As the annealing temperature increased, the hydroxyl groups were converted into oxide lattices. This fact has been confirmed by the results of XPS. Simultaneously, the V_T shifts to negative direction as the annealing temperature increased. It may be related with the significant carrier concentrations and oxygen vacancies in the HIZO active layer which was created by the high annealing temperature. Eventually, as shown in figure S5, the HIZO TFTs with HfSiOx dielectrics annealed at 500 °C showed a small counter-clockwise hysteresis which was caused by the still existed hydroxyl-groups as shown in figure S3 (b).

Compared with the TFT characteristics with HfO_2 and HfSiOx dielectrics annealed at 500 °C (Figure 6a), the HfSiOx dielectric TFTs had a relative low off-state current. This may be attributed to the amorphous phase of HfSiOx films, while the HfO_2 films were crystallized annealed at 500 °C which would contribute to electrical leakage current. In the case of mobile display/electronics, the off-state current should be kept to a minimum because it adversely affects the power consumption. On one hand, high leakage current has a detrimental effect on transistor performance, resulting in high off-state currents, low on/off ratios [8]. On the other hands, the energy ban gap was enlarged through the Si addition into HfO_2 dielectric, and this would increase the band offset between dielectrics and semiconductors, and then decrease the carriers injected into gate dielectrics.

Figure 6b showed the output characteristics of HIZO TFTs with HfSiOx dielectrics, a clear pinch-off suggested that electron transport in the HIZO active channel layer was controlled by gate and drain voltages. In addition, the absence of crawling in the drain current (I_{DS}) in the low drain voltage (V_{DS}) region suggested ohmic contact between the HIZO channel and ITO source/drain electrodes. Figure S6 showed the output characteristics of HIZO TFTs with HfSiOx dielectrics annealed at 300 °C (a) and HfO_2 dielectrics annealed at 500 °C (b). The HIZO TFTs on HfO_2 dielectrics had higher saturation current than that of HIZO TFTs on HfSiOx dielectrics, which may be due to the high capacitance of HfO_2 films. The HIZO TFTs with HfSiOx annealed at 300 °C exhibited a relative low saturation current, which may be related with the poor dielectric/channel interface affected by residual impurities and hydrogen groups.

Although we successfully demonstrated a solution processed TFTs with HfSiOx dielectrics and HIZO channel layer, the saturation mobility is still need to be improved. The earlier studies by demonstrated that the sputtered ZTO TFTs could achieve high mobility (~30 cm^2/(V s)) for the TFTs [29]. Thus, to further improve the TFTs mobility and verify the application of HfSiOx solution processed dielectrics. TFTs with HfSiOx dielectrics and ZTO channel layers were fabricated. Figure S7 showed the transfer characteristics of ZTO TFTs annealed at 500 °C. The ZTO TFTs showed a low threshold voltage of -0.53 V, a high saturation mobility of 153 cm^2/V·s, a subthreshold swing of 0.17 V/dec, an on-off current ratio 3.40×10^7. The small *S.S* values indicated that the TFTs have an excellent interface between dielectrics and semiconductors. Both the results of HIZO and ZTO TFTs prove that the solution processed HfSiOx dielectrics is an excellent dielectric candidate used in TFTs.

Conclusions

This research investigated the solution processed HfSiOx films affords smooth, amorphous dielectric material with high energy band gap, high capacitance and good insulating properties. The 500 °C annealed HfSiOx films showed a low leakage current of 10^{-7} at 1MV/cm, high breakdown voltage of 2.9 MV/cm, which can satisfy the need of TFTs industry. The solution processed HIZO TFTs exhibited low off-state current of 10^{-11} A, which indicated the effects of silicon oxide incorporation for reducing the leakage current. And the solution processed HIZO TFTs with HfSiOx dielectrics exhibited a saturation mobility of 6.11 cm^2/V·s, a low threshold voltage of -1.44 V, a small subthreshold swing of 0.55 V/dec and an on-off current ratio 6.14 ×10^5. Furthermore, the ZTO TFTs showed a high saturation mobility of 153 cm^2/V·s, a low threshold voltage of -0.53 V, a small subthreshold swing of 0.17 V/dec, a large on-off current ratio 3.4×10^7. All the results indicated that the solution processed HfSiOx dielectrics was an attractive candidate dielectric for low cost, high performance thin film transistors.

Acknowledgementsee

This work was supported by Shanghai science and technology commission under grant No13520500200 and 14XD1401800.

Notes and references

1 K. Nomura, H. Ohta, A. Takagi, T. Kamiya, M. Hirano and H. Hosono, *Nature*, 2004, **432**, 488-492.
2 X. F. Li, Q. Li, E. L. Xin and J. H. Zhang, *J. Sol-Gel Sci. Technol.*, 2013, **65**, 130-134.

Journal of Materials Chemistry C Accepted Manuscript

3 G. M. Huang, L. Duan, G. F. Dong, D. Q. Zhang and Y. Qiu, *ACS Appl. Mater. Interfaces*, 2014, **6**, 20786-20794.
4 Y. B. Yoo, J. H. Park, K. H. Lee, H. W. Lee, K. M. Song, S. J. Lee and H. K. Baik, *J. Mater. Chem. C*, 2013, **1**, 1651-1658.
5 X. F. Li, E. L. Xin and J. H. Zhang, *IEEE Trans. Electron Devices*, 2013, **60**, 3413-3416.
6 J. Peng, C. H. Sheng, J. F. Shi, X. F. Li and J. H. Zhang, *J. Sol-Gel Sci. Technol.*, 2014, **71**, 458-463.
7 L. Zhang, J. Li, X. W. Zhang, X. Y. Jiang and Z. L. Zhang, *Appl. Phys. Lett.*, 2009, **95**, 072112.
8 J. F. Martinez Hardigree, T. J. Dawidczyk, R. M. Ireland, G. L. Johns, B.-J. Jung, M. Nyman, R. Osterbacka, N. Markovic and H. E. Katz, *ACS Appl. Mater. Interfaces*, 2013, **5**, 7025-7032.
9 E. Fortunato, P. Barquinha and R. Martins, *Adv. Mater.*, 2012, **24**, 2945-2986.
10 X. F. Li , L. Y. Zhu, Y. N. Gao and J. H. Zhang, *IEEE Trans. Electron Devices*, 2015, **62**, 875-881.
11 Y. N. Gao, X. F. Li, L. L. Chen, J. F. Shi, X. W. Sun and J. H. Zhang, *IEEE Electron Device Lett.*, 2014, **35**, 554-556.
12 K. Jieun, K. Joohee, P. Si Yun, L. Eungkyu, K. Kyongjun, L. Keon-Hee and K. Youn Sang, *J. Mater. Chem. C*, 2014, **2**, 1050-1056.
13 D. Cho, S. Woo, J. Yang, D. Lee, Y. Lim, D. Kim, S. Park and M. Yi, *Electron. Mater. Lett.*, 2013, **9**, 381-384.
14 T. A. Naoi, H. Paik, M. L. Green and R. B. van Dover, *Journal of Advanced Dielectrics*, 2015, **05**, 1550010.
15 S. Kim, M.-H. Ham, J.-W. Lee, W. Lee and J.-M. Myoung, *Appl. Surf. Sci.*, 2008, **254**, 3943-3948.
16 K. Chang, K. Shanmugasundaram, J. Shallenberger and J. Ruzyllo, *Thin Solid Films*, 2007, **515**, 3802-3805.
17 L. Seunghyup, Y. Dong-Jin, R. Shi-Woo and Y. Kijung, *J. Mater. Chem.*, 2009, **19**, 6857-6864.
18 K. Xiong, Y. Du, K. Tse and J. Robertson, *J. Appl. Phys.*, 2007, **101**, 024101.
19 G. He, L. D. Zhang, G. W. Meng, G. H. Li, G. T. Fei, X. J. Wang, J. P. Zhang, M. Liu, Q. Fang and I. W. Boyd, *J. Appl. Phys.*, 2008, **104**, 104116.
20 H. Hau-Yuan, W. Shui-Jinn, W. Chien-Hung, C. Chen-Kuo, H. Yen-Chieh and S. Je-Yi, *Applied Physics Express*, 2010, **3**, 121501.
21 W. Yang, M. Fronk, Y. Geng, L. Chen, Q.-Q. Sun, O. D. Gordan, P. zhou, D. R. T. Zahn and D. W. Zhang, *Nanoscale Research Letters*, 2015, **10**, 32.
22 H. K. Kim, H.-S. Jung, J. H. Jang, J. Park, T. J. Park, S.-H. Lee and C. S. Hwang, *J. Appl. Phys.*, 2011, **110**, 114107.
23 X. Cheng, Z. Song, J. Jiang, Y. Yu, W. Yang and D. Shen, *Appl. Surf. Sci.*, 2006, **252**, 8073-8076.
24 L. Yue, H. F. Pu, H. L. Li, S. J. Pang and Q. Zhang, *J. Phys. D: Appl. Phys.*, 2013, **46**, 445106.
25 J. W. Hennek, Y. Xia, K. Everaerts, M. C. Hersam, A. Facchetti and T. J. Marks, *ACS Appl. Mater. Interfaces*, 2012, **4**, 1614-1619.
26 C. M. McGilvery, S. De Gendt, E. A. Payzant, M. MacKenzie, A. J. Craven and D. W. McComb, *J. Am. Ceram. Soc.*, 2012, **95**, 3985-3991.
27 X. M. Yang, T. Yu, X. M. Wu, L. J. Zhuge, S. B. Ge and J. J. He, *Appl. Surf. Sci.*, 2011, **257**, 9277-9281.
28 E. Talbot, M. Roussel, C. Genevois, P. Pareige, L. Khomenkova, X. Portier and F. Gourbilleau, *J. Appl. Phys.*, 2012, **111**, 103519.
29 R. L. Hoffman, *Solid-State Electron*. 2006, **5**, 784−787.
30 Y. J. Kim, S. Oh, B. S. Yang, S. J. Han, H. W. Lee, H. J. Kim, J. K. Jeong, C. S. Hwang and H. J. Kim, *ACS Appl. Mater. Interfaces*, 2014, **6**, 14026-14036.
31 S. J. Kim, H.-J. Jeon, S.-J. Oh, S. S. Lee, Y. Choi, J.-S. Park and S. Jeong, *ACS Appl. Mater. Interfaces*, 2014, **6**, 18429-18434.
32 J. H. Park, Y. B. Yoo, K. H. Lee, W. S. Jang, J. Y. Oh, S. S. Chae and H. K. Baik, *ACS Appl. Mater. Interfaces*, 2013, **5**, 410-417.
33 L. Y. Zhu, Y. N. Gao, X. F. Li, X. W. Sun and J. H. Zhang, *J. Mater. Res.*, 2014, **29**, 1620-1625.
34 A. Toriumi, K. Kita, K. Tomida and Y. Yamamoto, *ECS Trans.*, 2006, **1**, 185-197.
35 K. Jang, J. Raja, J. Kim, C. Park, Y.-J. Lee, J. Yang, H. Kim and J. Yi, *Semicond. Sci. Technol.*, 2013, **28**, 085015.
36 W. Xu, H. Wang, F. Xie, J. Chen, H. Cao and J.-B. Xu, *ACS Appl. Mater. Interfaces*, 2015, **7**, 5803-5810.
37 K.-H. Lim, K. Kim, S. Kim, S. Y. Park, H. Kim and Y. S. Kim, *Adv. Mater.*, 2013, **25**, 2994-3000.
38 M. Jerman, Z. H. Qiao and D. Mergel, *Appl. Opt.*, 2005, **44**, 3006-3012.
39 D. Mergel, D. Buschendorf, S. Eggert, R. Grammes and B. Samset, *Thin Solid Films*, 2000, **371**, 218-224.
40 W. Yang, M. Fronk, Y. Geng, L. Chen, Q.-Q. Sun, O. D. Gordan, P. zhou, D. R. T. Zahn and D. W. Zhang, *Nanoscale Research Letters*, 2015, **10**, 32.
41 C. V. Ramana, G. Baghmar, E. J. Rubio and M. J. Hernandez, *ACS Appl. Mater. Interfaces*, 2013, **5**, 4659-4666.
42 D. Cao, X. Cheng, Y. Yu, X. Li, C. Liu, D. Shen and S. Mändl, *Appl. Phys. Lett.*, 2013, **103**, 081607.
43 P. Punchaipetch, G. Pant, M. A. Quevedo-Lopez, C. Yao, M. El-Bouanani, M. J. Kim, R. M. Wallace and B. E. Gnade, *IEEE J. Sel. Top. Quantum Electron.*, 2004, **10**, 89-100.
44 Y. J. Kim, B. S. Yang, S. Oh, S. J. Han, H. W. Lee, J. Heo, J. K. Jeong and H. J. Kim, *ACS Appl. Mater. Interfaces*, 2013, **5**, 3255-3261.
45 P. N. Plassmeyer, K. Archila, J. F. Wager and C. J. Page, *ACS Appl. Mater. Interfaces*, 2015, **7**, 1678-1684.
46 J. H. Park, J. Y. Oh, S. W. Han, T. I. Lee and H. K. Baik, *ACS Appl. Mater. Interfaces*, 2015, **7**, 4494-4503.
47 J.-W. Jo, J. Kim, K.-T. Kim, J.-G. Kang, M.-G. Kim, K.-H. Kim, H. Ko, Y.-H. Kim and S. K. Park, *Adv. Mater.*, 2015, **27**, 1182-1188.

Journal of Materials Chemistry C Accepted Manuscript

This journal is © The Royal Society of Chemistry 20xx